Journal Pre-proof

Preclinical study of additive manufactured plates with shortened lengths for complete mandible reconstruction: Design, biomechanics simulation, and fixation stability assessment

Qimin Shi, Yi Sun, Shoufeng Yang, Jeroen Van Dessel, Heinz-Theo Lübbers, Shengping Zhong, Yifei Gu, Michel Bila, Constantinus Politis

PII: S0010-4825(21)00802-7

DOI: https://doi.org/10.1016/j.compbiomed.2021.105008

Reference: CBM 105008

To appear in: *Computers in Biology and Medicine*

Received Date: 8 August 2021

Revised Date: 29 October 2021

Accepted Date: 29 October 2021

Please cite this article as: Q. Shi, Y. Sun, S. Yang, J. Van Dessel, H.-T. Lübbers, S. Zhong, Y. Gu, M. Bila, C. Politis, Preclinical study of additive manufactured plates with shortened lengths for complete mandible reconstruction: Design, biomechanics simulation, and fixation stability assessment, *Computers in Biology and Medicine* (2021), doi: https://doi.org/10.1016/j.compbiomed.2021.105008.

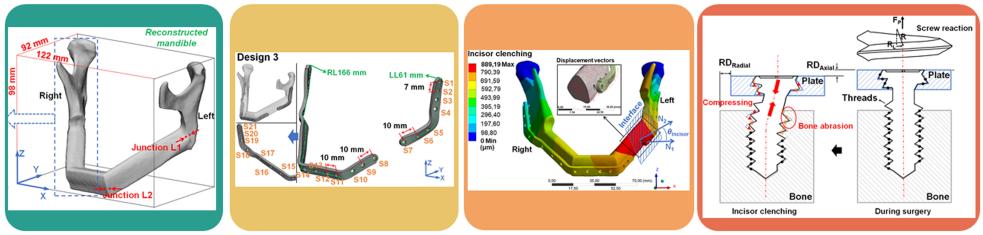

Reconstructed mandible using CT data → Design of short plates combination → Biomechanics simulation of stress/ displacement → Fixation stability analysis

Preclinical study of additive manufactured plates with shortened lengths for complete mandible reconstruction: Design, biomechanics simulation, and fixation stability assessment

Qimin Shi[1], Yi Sun[1]*, Shoufeng Yang[2]*, Jeroen Van Dessel[1], Heinz-Theo Lübbers[3,4], Shengping Zhong[1], Yifei Gu[1], Michel Bila[1], Constantinus Politis[1]

1. KU Leuven, Department of Biomedical Sciences, OMFS-IMPATH Research Group & UZ Leuven (University Hospitals Leuven), Oral and Maxillofacial Surgery, Kapucijnenvoer 33, 3000 Leuven, Belgium

2. University of Southampton, Faculty of Engineering and Physical Sciences, Southampton SO17 1BJ, UK

3. University Hospital of Zurich, Clinic for Cranio-Maxillofacial Surgery, Frauenklinikstrasse 24, Zurich CH-8091, Switzerland

4. Harvard Medical School, Brigham and Women's Hospital, Surgical Planning Laboratory, Francis Street 75, Boston, MA 02115, USA

*Corresponding authors.

E-mail addresses: yi.sun@uzleuven.be (Y. Sun); shoufeng.yang@gmail.com (S. Yang)

Abstract

Background: A combination of short titanium plates fabricated using additive manufacturing (AM) provides multiple advantages for complete mandible reconstruction, such as the minimisation of inherent implant deformation formed during AM and the resulting clinical impact, as well as greater flexibility for surgical operation. However, the biomechanical feasibility of this strategy is still unclear, and therefore needs to be explored.

Method: Three different combinations of short mandible reconstruction plates (MRPs) were customised considering implant deformation during the AM process. The resulting biomechanical performance was analysed by finite element analysis (FEA) and compared to a conventional single long MRP.

Results: The combination of a long plate and a short plate (Design 3 [LL61 mm/RL166 mm]) shows superior biomechanical properties to the conventional single long plate (Design 1 [TL246 mm]) and reveals the most reliable fixation stability among the three designs with short plates. Compared to conventional Design 1, Design 3 provides higher plate safety (maximum tensile stress on plates reduced by 6.3%), lower system fixation instability (relative total displacement reduced by 41.4%), and good bone segment stability (bone segment dislocation < 42.1 μm) under masticatory activities.

Conclusions: Preclinical evidence supports the biomechanical feasibility of using short MRPs for complete mandible reconstruction. Furthermore, the results could also provide valuable information when treating other large-sized bone defects using short customised implants, expanding the potential of AM for use in implant applications.

Keywords: Finite element analysis (FEA); Additive manufacturing (AM); Patient-specific customised implants (PSCIs); Mandible reconstruction; Biomechanics

1. Introduction

Selective laser melting (SLM), one of the promising metal additive manufacturing (AM; interchangeably called 3D printing) techniques, has been widely used to create patient-specific customised implants (PSCIs) in orthopaedic [1], craniomaxillofacial [2], and dental [3, 4] applications. SLM is used to fabricate an implant in a revolutionary additive manner (point-by-point, line-by-line, and layer-by-layer) starting from metal powders, allowing sufficient design freedom to produce PSCIs that would otherwise be challenging or even impossible to fabricate through conventional subtractive or formative techniques [5]. The good mechanical and biomechanical performance of SLM-fabricated PSCIs has been well documented. The use of a fine laser beam (spot diameter of 30-100 μm) and a thin powder layer thickness (typically below 100 μm) allows SLM to produce customised implants with high precision [5]. An implant geometry strongly matched to the patient's anatomical structure improves the implant placement precision, shortens the recovery and rehabilitation process, allows optimum reconstruction of joint kinetics, enhances implant fixation stability, and results in fewer postoperative infections [6, 7]. In addition, the short interaction between the laser beam and powder bed enables the powder system to experience a rapid heating/cooling process, leading to fine and uniform metallurgical microstructures and improved mechanical properties [8]. Biomechanically, the improved mechanical properties, particularly the fatigue strength and yield strength, can extend the implant lifespan without premature fatigue crack initiation and plastic deformation [9].

Although SLM-fabricated PSCIs have a great reputation in biomedical applications, the non-uniform heat input under its inherent domain-by-domain localised formation tends to produce high tensile residual stress on the implant. The tensile residual stress not only accelerates fatigue crack growth under cyclic loading but also causes macroscale implant deformation, reducing implant placement precision [10, 11]. Such implant deformation is particularly significant in bar-like structures due to relatively large stress accumulation along the length compared with that oriented along the thickness and width [12]. To avoid unfavourable part deformation, a stress-relieving heat treatment is usually applied before the printed parts are cut from the base plate. However, the plastic deformation that usually occurs at the ends of the bar-like structures cannot be recovered by subsequent heat treatment, influencing the final implant structure. In fact, bar-like structures are required in many biomedical applications, especially the plates for mandible reconstruction, as they reduce the implant exposure potential by minimising the implant thickness and width [13].

As the initial step of the AM process, the implant design can be fundamental to optimising the stress distribution on the implant and thus mitigating the implant deformation [14]. More importantly, the biomedical properties of implants, such as high fixation stability [15], good biomechanics [16], lightweight [17], and desired bone/nerve/tissue regeneration capability [18-20], are closely associated with the implant geometry. Therefore, the need to minimise implant deformation and optimise biomedical properties is driving researchers to remodel the conventional implant structure. For bar-like implants, shortening the length can be the most straightforward solution to lowering the tensile residual stress and minimising implant deformation. Clinically, the shortened PSCIs have numerous advantages: higher flexibility for surgical operation and lower difficulty of implant placement. Furthermore, the reduced contact area between the short implants and the bone surface leaves fewer biological footprints on the periosteum, which guarantees smooth nutrition transportation through the periosteum to the bone and thus benefits bone recovery and rehabilitation [21].

Recently, Palka et al. [15] studied the biomechanical feasibility of using shortened plates from SLM to treat a small-sized mandible fracture of several millimetres. They designed novel modular star-like plates (diameter of 10 mm) and matched dog-bone-like plates (length of 19 mm) to replace a long, flat, bar-like plate (length of about 25 mm). The subsequent biomechanics simulation by finite element analysis (FEA) showed good construction stability on the treated bone, benefiting bone segment stability, anatomic gap reduction, and physiological bone function restoration.

However, whether the shortened implants can be used to treat large-sized bone defects is unclear. Therefore, this work was performed based on a case study of complete mandible reconstruction with fibula graft. Mandible defects of this extent usually occur after mandible resection due to tumours, osteoradionecrosis, and medication-related osteonecrosis of the jaw [22]. When the size of a mandible defect spans tens of centimetres, mandible reconstruction plates (MRPs) are deemed necessary to reconstruct mandible functionality. As illustrated in Fig. 1, four designs of MRPs were customised, including a conventional design (Design 1) and three new designs consisting of short plates (Designs 2–4). Implant deformation was predicted by an SLM process simulation to assist implant design. By performing FEA, the safety and fixation stability of the short MRPs for mandible reconstruction was evaluated. The objective of this work was to preclinically assess whether customised short MRPs prepared by SLM can be feasible to treat large-sized mandible bone defects compared to the gold-standard long MRPs.

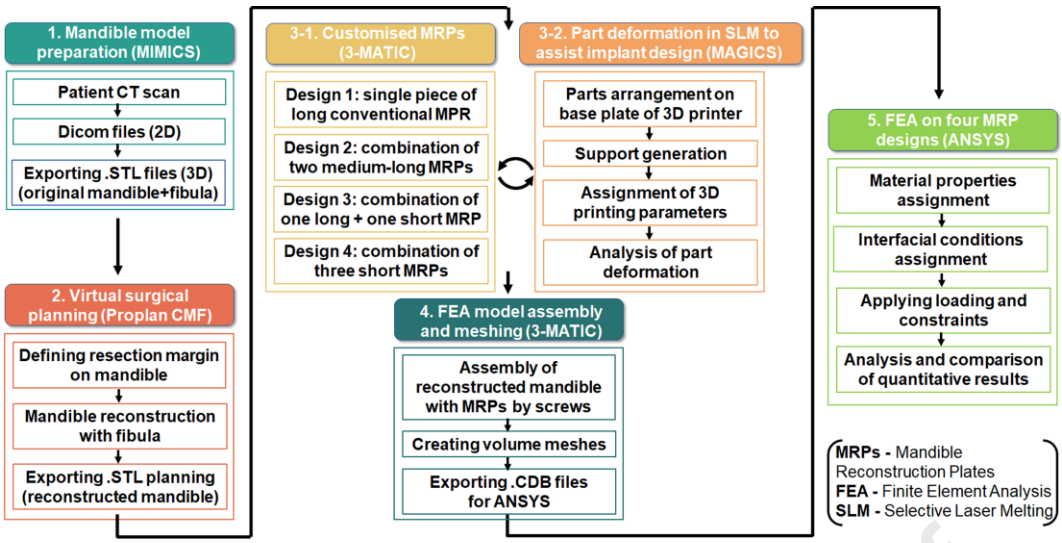

Fig. 1. Flowchart of biomechanics simulation on customised MRPs.

2. Materials and methods

2.1 Patient history and virtual planning

A 58-year-old male patient was treated at the Department of Oral & Maxillofacial Surgery, UZ Leuven, Belgium, for complete mandible reconstruction with tumour resection. A high-resolution CT scan of the craniofacial skeleton and fibula was obtained preoperatively using an in-plane resolution of 0.75 mm² and a slice thickness of 1 mm. CT data was post-processed and segmented in Mimics v22.0 (Materialise, Leuven, Belgium). Then, the segmented models were imported into Proplan CMF software (Materialise, Leuven, Belgium) for virtual surgical planning. The reconstructed mandible had a global dimension of 122 mm × 92 mm × 98 mm (length × width × height) with three fibula pieces (Fig. 2). Clinically, the chewing activities of the patient are strictly restricted at the initial stage after the mandible reconstruction to guarantee bone recovery. Therefore, this study was performed assuming the bone system is at the late rehabilitation stage. At this stage, osseointegration has almost completed, and loading can be transferred between the mandible and the fibulas. Thus, the fibulas were merged with the retained mandible for the subsequent FEA. To evaluate the bone segment stability provided by the customised MRPs, the mandible segment dislocation was assessed during the biomechanics simulation. The mandible segment dislocation was obtained by comparing the relative displacement at the two sides of a bone junction with a distance of 2.5 mm (Junctions L1, L2, L3, and L4 in Fig. 2).

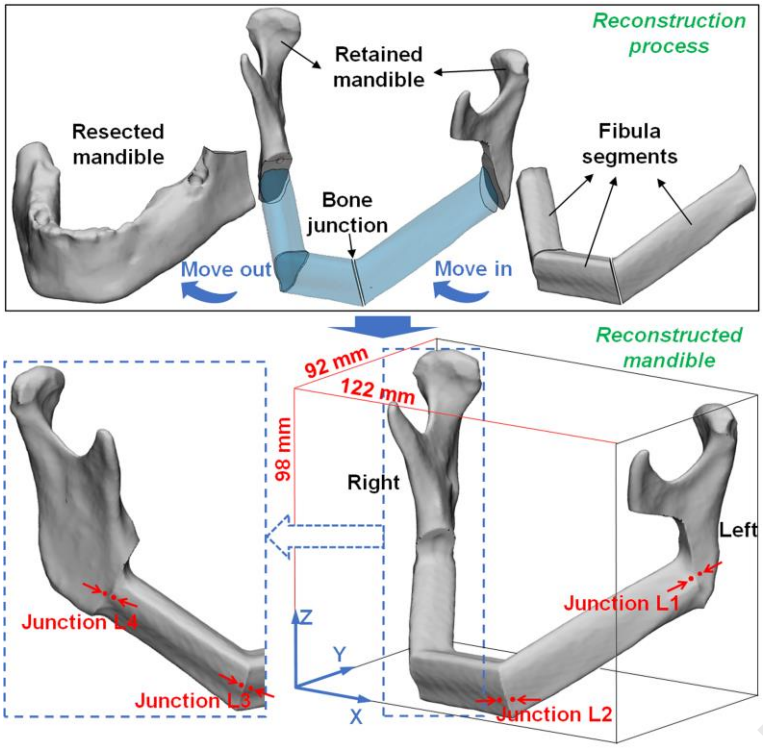

Fig. 2. Mandible reconstruction process and the reconstructed mandible.

2.2 Mandible reconstruction plate (MRP) design process

Four different patient-specific customised MRPs were designed in 3-Matic v14.0 (Materialise, Leuven, Belgium) based on the reconstructed mandible (Fig. 3). All designs have a thickness of 2.5 mm and a height of 7 mm. Design 1 is a single, long conventional MPR (total plate length of 246 mm, termed as [TL246 mm]; Fig. 3a), and Design 2 consists of two medium-long plates (left plate length of 119 mm and right plate length of 121 mm, termed as [LL119 mm/RL121 mm]; Fig. 3b). Design 3 consists of one long and one short plate (left plate length of 61 mm and right plate length of 166 mm, termed as [LL61 mm/RL166 mm]; Fig. 3c), and Design 4 consists of three short plates (right plate length of 61 mm, middle plate length of 91 mm and right plate length of 67 mm, termed as [RL61 mm/ML91 mm/RL67 mm]; Fig. 3d). Clinical recommendations call for three or four screws on the side of a plate to provide adequate fixation stability [23]. Following this recommendation, four screw holes with 7 mm spacing were assigned at the condyle end of the plate, as the highest stress is expected to accumulate at that location under masticatory activities [10]. In contrast, two or three screw holes with a spacing of 10 mm were arranged at the chin end of the plate as they are exposed to relatively lower stress, with a greater distance of 15 mm between screw holes in the middle of the plate. The screw hole had a diameter of 3 mm. With designs using two or three short plates, the total number of necessary screw holes increased from 18 in Design 1 to 24 in Design 4.

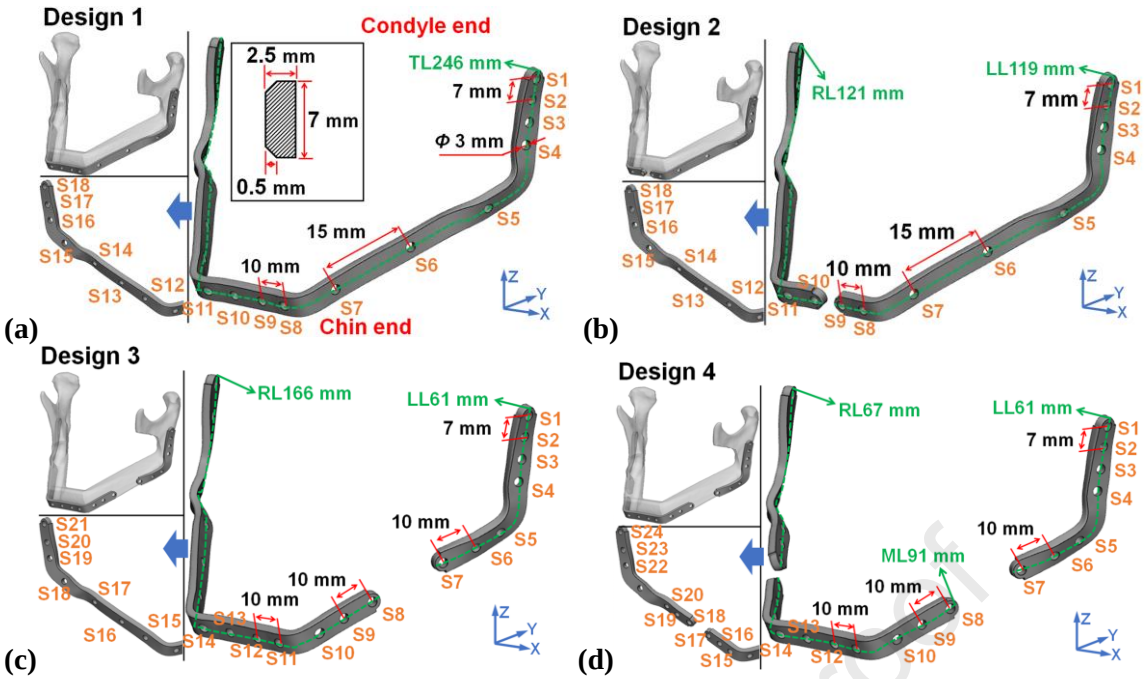

Fig. 3. Models of patient-specific customised MRPs: (a) Design 1, (b) Design 2, (3) Design 3 and (4) Design 4. (S1–S24 highlight the position and number of screw holes on the MRPs.)

2.3 Implant deformation evaluation and in vitro experimental validation

Magics v25.01 (Materialise, Leuven, Belgium) was used to simulate the SLM process and evaluate the implant deformation that can occur during the SLM. Each customised MRP was placed on the base plate first. Afterwards, removable support structures that assist the building of overhang structures during the SLM were generated (Fig. 4). The implant deformation simulation followed the guidelines and settings suggested by Materialise: ε_x = -0.004415, ε_y = -0.004457, ε_z = -0.019426, and layer thickness = 30 µm. A voxel size of 0.5 mm × 0.5 mm × 0.4 mm (X × Y × Z) was used to achieve both simulation efficiency and precision. The building orientation of the MRPs and subsequent support generation were selected considering the optimal printing condition of titanium and the quality requirement for the MRPs. For example, the upper surface quality of the MRPs should be prioritised during the SLM to guarantee fatigue performance, since a fatigue crack is highly likely to initiate from the upper surface due to high tensile stress [10]. Therefore, the building of the MRPs during the SLM started from the chin end and ended at the condyle end, and the entire support structure was generated on the bottom surface of the MRPs (Fig. 4). In addition, screw holes on the MRPs were drilled and tapped after the SLM process using a computer numerical control (CNC) machine to achieve processing quality, so there were no screw holes on the MRPs during the SLM.

The designed MRPs were then printed by a TruPrint 1000 SLM machine to evaluate the printability of the model. The machine is equipped with a 200 W TRUMPF fibre laser, producing a laser beam with a wavelength of 1070 nm and a diameter of 55 µm in a continuous mode. Ti-6Al-4V powder with a size

distribution of 15-45 μm and an average diameter of 30 μm was used as the raw material. The suggested laser parameters by the manufacturer were applied, allowing a volumetric energy density of 56 J/mm^3 to be achieved. In addition, the reconstructed mandible model was prepared using a Stratasys Connex 350 3D printer using polymer material. Then, the metal implants were fixed onto the mandible model in order to check the geometrical suitability between the mandible and the implants preclinically. It should be noted that the MRPs and the corresponding mandible model were scaled down using a factor of 0.7 to match the building chamber size of the SLM machine.

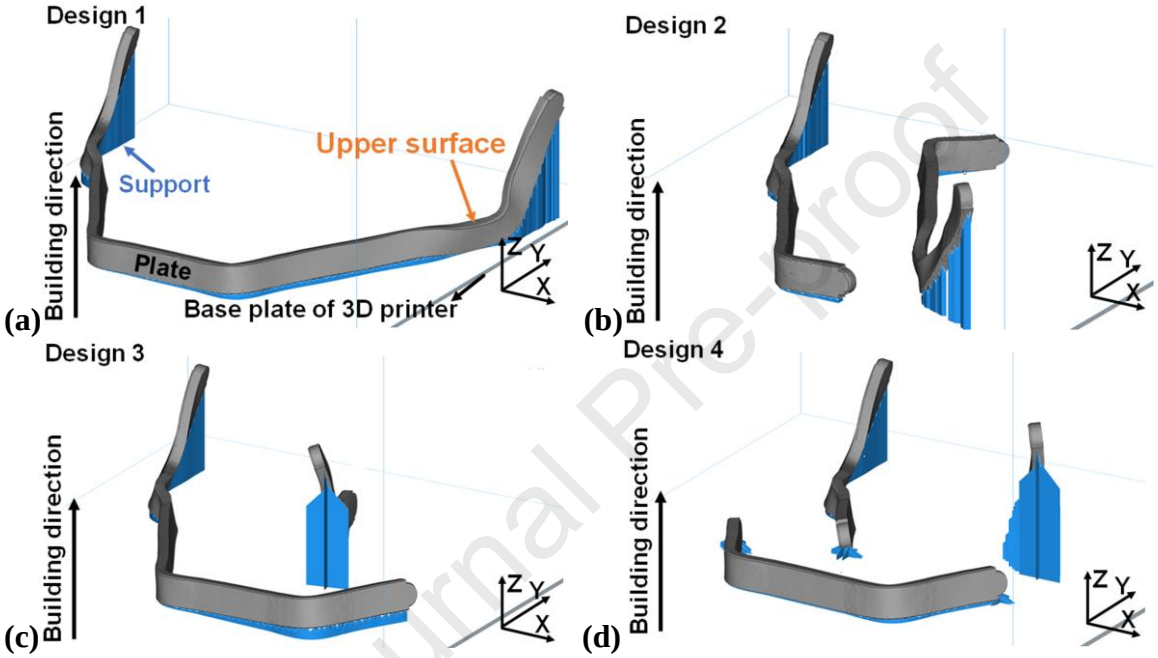

Fig. 4. Building arrangement of MRPs on the base plate of the SLM 3D printer with support structures: (a) Design 1, (b) Design 2, (3) Design 3, and (4) Design 4. (Screw holes on the MRPs were drilled and tapped after the SLM process by a CNC machine to provide processing quality.)

2.4 Finite element analysis (FEA) of biomechanical behaviours

Finite element analysis (FEA) simulating human masticatory activities was performed using an ANSYS Workbench static structural analysis package and used to understand the biomechanical behaviour of the customised MRPs, such as stress distribution and displacement. The FEA process included assembling the FEA model, meshing, assigning material properties, assigning interfacial conditions, and loading muscle forces and constraints. The FEA model assembly and meshing were prepared in 3-Matic software before being imported into ANSYS Workbench.

2.4.1 FEA model assembly

The FEA model assembly consisted of the customised MRP(s) attached to the reconstructed mandible and titanium screws (Fig. 5). This work mainly focused on the overall fixation feasibility enabled by the customised short MRPs from SLM. Therefore, the analysis used a simplified cylinder shape (diameter of 3

mm and length of 10 mm) for the screws to improve calculation efficiency. Similarly, the dental part was simplified and not included in the model. The coordinate origin of the model assembly was located at the physical geometrical centre; the X-axis, Y-axis, and Z-axis were assigned from the right temporomandibular joint (TMJ) to the left TMJ, from the forehead end to the afterbrain end, and from the neck end to the skull end, respectively.

2.4.2 Meshing

Considering the ease and robustness of the four-node tetrahedral (Tet4) volume element, this study adopted Tet4 in all the components (Fig. 5). A fine Tet4 volume element size with a maximum edge length of 1.0 mm was utilised in the MRPs and screws, and relatively coarse Tet4 volume elements (maximum edge length of 3.0 mm) were adopted in the large-sized mandible to provide a balance between computational precision and numerical simulation efficiency. Four model assemblies were meshed into 165790–177494 elements and 36990–39134 nodes.

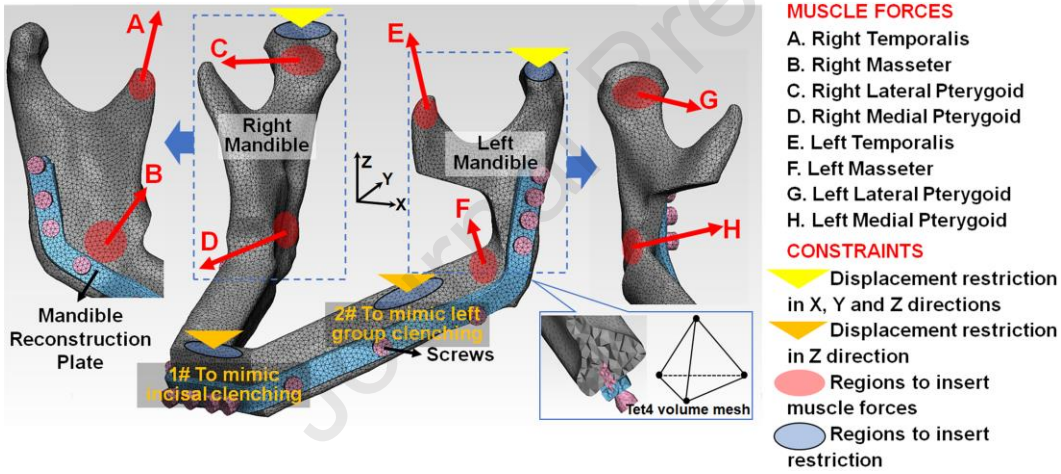

Fig. 5. Three-dimensional finite element analysis (FEA) model for simulating human masticatory activities. (Red arrows highlight muscle insertions and direction.)

2.4.3 Material parameters

Ti-6Al-4V was selected as the material of the MRPs and screws based on its clinical usability and biocompatibility. The plate and screws were considered to be defect-free to exclude any influence of material metallurgical defects in the biomechanics simulation. A heat treatment is usually applied after the SLM process for titanium alloys in order to release residual stress and achieve isotropic mechanical properties by consuming epitaxial columnar grains [24, 25]. Thus, the Ti-6Al-4V material properties were assigned to be linear-elastic, isotropic, and homogeneous: Young's modulus = 113800 MPa, Poisson's ratio = 0.34, fatigue strength = 510 MPa, and yield strength = 870 MPa [26-28].

Modelling bone tissue can be a demanding task due to its heterogeneous structure with cortical and trabecular bones. Thus, the bone model in the FEA is usually simplified to a greater or lesser extent. The bone model in this work was simplified to be a dense cortical bone based on three considerations [26, 29, 30]. First, Andersen et al. [31] highlighted that the optimisation of bone structure features does not significantly influence the biomechanical results, due to the comparatively small volume of the medullary cavity compared to the whole mandible volume. This finding enabled the simplification of the mandible into a uniform cortical tissue. Second, the screws in this work are long enough to be inserted throughout the fibula, providing a stable fixation of the screw in the bone; thus, the loading can be transferred stably and smoothly from the mandible to the plate. Therefore, there was minimal influence of the removal of the medullary cavity on biomechanical behaviours. Third, the use of a simplified model improves the simulation efficiency by avoiding convergence difficulties caused by complex features in the model, such as cavities. A smooth and fast FEA also benefits the implant design process for patients. The Young's modulus and Poisson's ratio of the reconstructed mandible were defined as 13700 MPa and 0.30, respectively [26].

2.4.4 Interface conditions

Locking plate/screw systems are widely used clinically for two reasons. First, the locking plate/screw system can enhance stability by locking the screw to the plate [32]. Second, locking plates are usually not compressed on the bone. Thus, the locking plate has fewer biological footprints on the periosteum, which benefits the recovery of transplanted fibulas [21]. Under the assumption of the locking plate/screw system, it was considered that there was no plane-to-plane contact and no stress interaction between the reconstructed mandible and the plate. The plate-screw interface was assigned to a 'bonded' contact condition to reflect the strong locked bonding. In addition, the screw-bone interface was assumed to be 'frictional' with a coefficient of 0.3 [33].

2.4.5 Muscle force loading and constraints

The FEA simulated the static loading conditions of incisor clenching (to evaluate the biomechanical difference on the two sides of the customised MRPs) and left molar clenching (to evaluate the biomechanics under extreme biting force). As shown in Fig. 5, two condyles were restricted in all three degrees of freedom (X-, Y-, and Z-directions). The region corresponding to incisor teeth on the mandible was restricted in the Z direction for the incisor clenching simulation, and the region corresponding to left molar teeth on the mandible was restricted in the Z direction for the left molar clenching simulation. Korioth and Hannam [34,

35] reported that three major muscle groups must be loaded to simulate human masticatory activities: masseter muscles, temporalis muscles, and pterygoid muscles. Pinheiro and Alves [26] calculated the muscle forces based on the desired biting forces for different masticatory activities of a healthy human, as summarised in Table 1. As this study was performed at the late rehabilitation stage, besides the complete osseointegration at bone junctions, the muscle tissues were expected to attach to the bone steadily to drive full muscle forces. Plus, using full muscle forces of healthy people allows a conservative evaluation of the implant safety and fixation stability, providing highly transferable information for the research community. Therefore, the calculated muscle forces of a healthy adult male were used in this work. Furthermore, note that after the mandibular region for the muscle attachment of the left masseter was partially resected (see Fig. 5), the left masseter muscle was attached to the corresponding region on the fibula clinically, to reconstruct the patient's full muscle activities. Thus, the left masseter was also considered in the FEA and loaded on the fibula. All these muscle forces were loaded on a set of nodes at the corresponding muscle insertion site (Fig. 5).

Table 1. Muscle forces for the masticatory activity of incisor clenching and left molar clenching.

Muscle groups	Muscle forces along X-, Y- and Z-directions (N)					
	Incisor clenching			Left molar clenching		
	X	Y	Z	X	Y	Z
Right masseter	-123.0	-109.4	375.4	-128.9	-80.8	356.9
Left masseter	123.0	-109.4	375.4	134.1	-22.3	304.8
Right temporalis	-17.0	22.0	84.3	-22.5	36.3	103.7
Left temporalis	17.0	22.0	84.3	225.4	383.2	1023.5
Right lateral pterygoid	183.8	-203.5	-32.4	44.3	-49.7	-8.7
Left lateral pterygoid	-183.8	-203.5	-32.4	-169.5	-194.8	-37.5
Right medial pterygoid	298.2	-228.9	485.3	374.5	-287.4	609.5
Left medial pterygoid	-298.2	-228.9	485.3	-34.5	-26.5	56.1

3. Results

3.1 Implant deformation during SLM and in vitro experimental validation

The implant deformation was determined as the relative displacement of a point on the model between its location after SLM and its original position (Fig. 6). The red-colour region in the figure highlights the large displacement. The SLM process is seen to produce various displacement values to different locations on the customised MRPs, leaving ununiform plate deformation. The maximum displacement value is always located at the highest location of a plate, which could be attributed to the thermal-stress accumulation layer by layer during the SLM [36]. With a decrease in plate length, the implant deformation can be reduced significantly by 30% to 59%, decreasing the maximum displacement to 1.5–2.6 mm (Designs 2–4; Fig. 6b–

d) from 3.7 mm (Design 1; Fig. 6a). A reduced implant deformation can improve the implant placement precision and thus benefit the clinical outcomes.

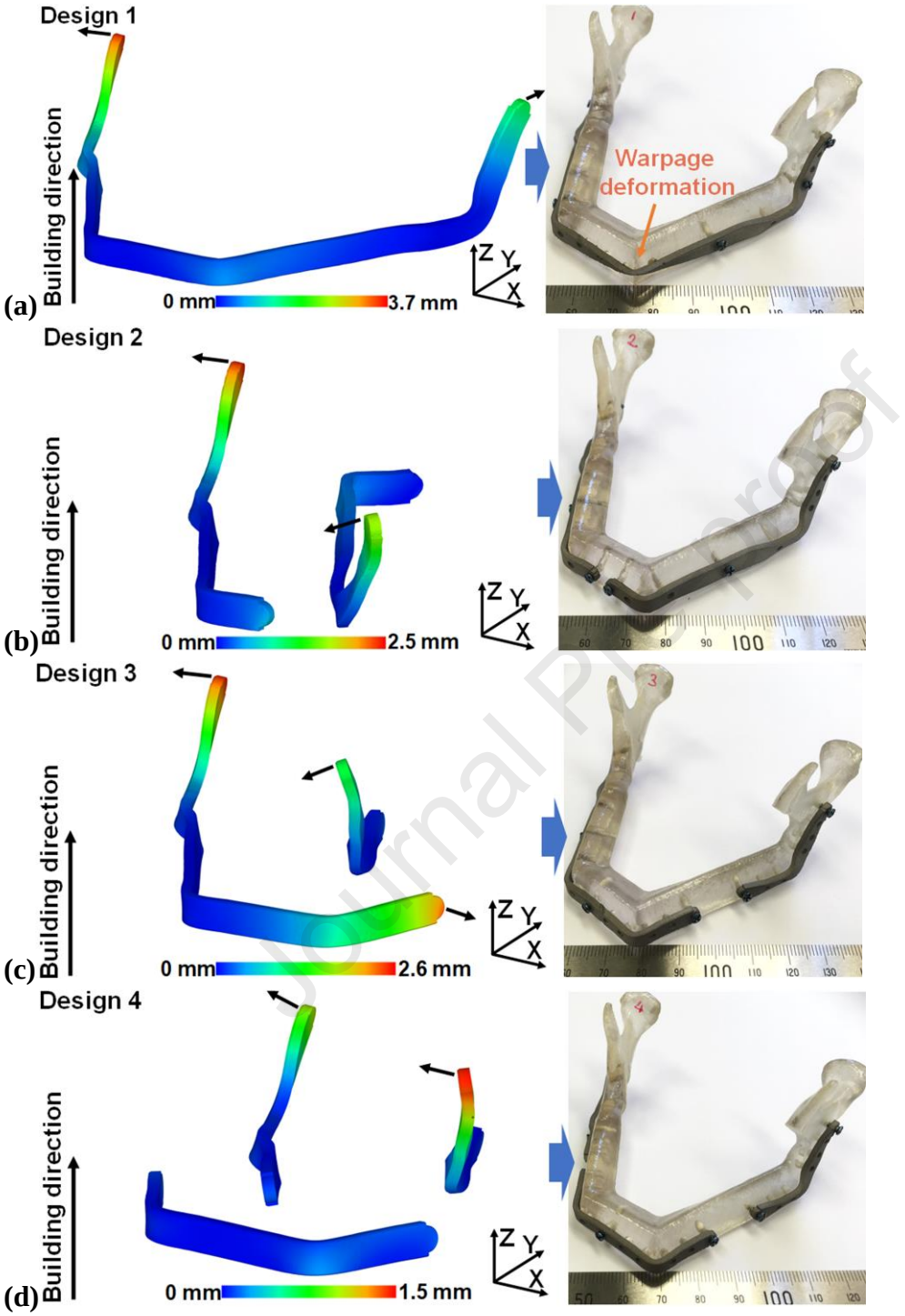

Fig. 6. Implant deformation prediction during SLM and in vitro experimental validation: (a) Design 1, (b) Design 2, (3) Design 3 and (4) Design 4. (Black arrows highlight the displacement direction. Screw holes on the MRPs were drilled and tapped after SLM by a CNC machine to provide processing quality, so there were no screw holes on the MRPs during the implant deformation prediction.)

The SLM-fabricated MRPs validate the plate deformation prediction. Obvious warpage deformation can be seen on Design 1 due to large stress concentration (Fig. 6a), suggesting the comparatively poor printability of a long plate in SLM. Although having slight plate deformation, the short plates in Designs 2–4

can be well manufactured by SLM and fixed onto the reconstructed mandible model (Fig. 6b–d). The geometrical suitability of the mandible and the metal plates, in turn, preclinically reflects the feasibility of using SLM to prepare patient-specific implants for complete mandible reconstruction.

3.2 Von Mises stress under masticatory activities

The subsequent biomechanics simulation was used to calculate the von Mises stress on the customised MRPs during incisor clenching and left molar clenching (Fig. 7 and Fig. 8, respectively). In general, tensile stress is seen on the whole plate in all cases. The minimum stress is observed on the chin end, and the maximum stress occurs near screw hole S5 (Design 1) or screw hole S4 (Designs 2–4). The higher stress on the left side compared to the right side under incisor clenching can be attributed to the resection of a larger bone volume on the original mandible above Junction L1 for this patient (Fig. 2), suggesting the critical role of bone volume in undertaking clenching loading. The importance of bone volume in mandible reconstruction has long been recognised clinically [37]. The higher risk of the left plate highlights the need to perform a biomechanics simulation of left molar clenching, for example, to evaluate the implant safety under extreme biting force.

During incisor clenching, Design 3 [LL61 mm/RL166 mm] shows the greatest capability of lowering the maximum stress, decreasing the stress to 144.9 MPa (Fig. 4c) from 154.61 MPa in Design 1 [TL246 mm], a decrease of 6.3% (Fig. 7a). Meanwhile, Design 4 [RL61 mm/ML91 mm/RL67 mm] only presents a slight decline of about 4 MPa in the maximum stress compared to Design 1 (Fig. 7d). In contrast, the two medium-long plates [LL119 mm/RL121 mm] in Design 2 increase the maximum stress to 183.2 MPa, an increase of 18.5% compared to Design 1 (Fig. 7b).

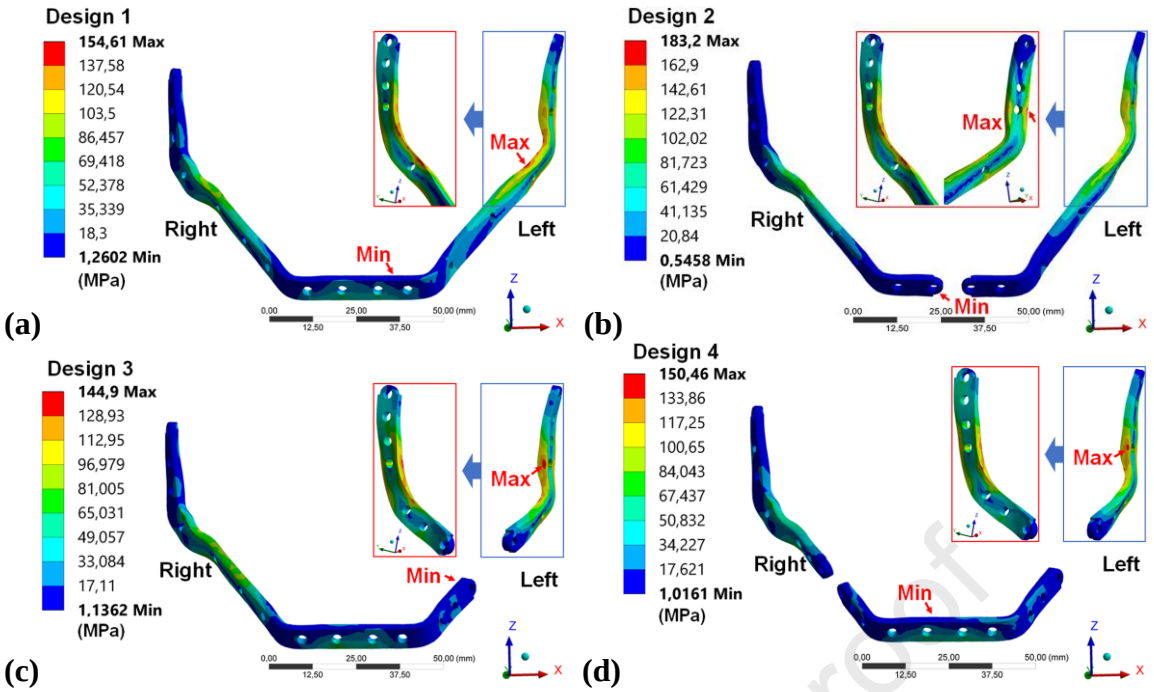

Fig. 7. Von Mises stress distribution on customised MRPs during incisor clenching: (a) Design 1, (b) Design 2, (3) Design 3, and (4) Design 4.

During left molar clenching, the maximum stress on the four designs ranges from 300.69 to 371.71 MPa. Different from incisor clenching, Design 4 [RL61 mm/ML91 mm/RL67 mm] produces the highest maximum stress among the four cases, increasing the maximum stress to 371.71 MPa (Fig. 8d) from 313.64 MPa on Design 1, an increase of 18.5% (Fig. 8a). Also, Design 3 [LL61 mm/RL166 mm] exhibits the lowest maximum stress (300.69 MPa; Fig. 8c), which is 4.1% lower than the maximum stress on Design 1.

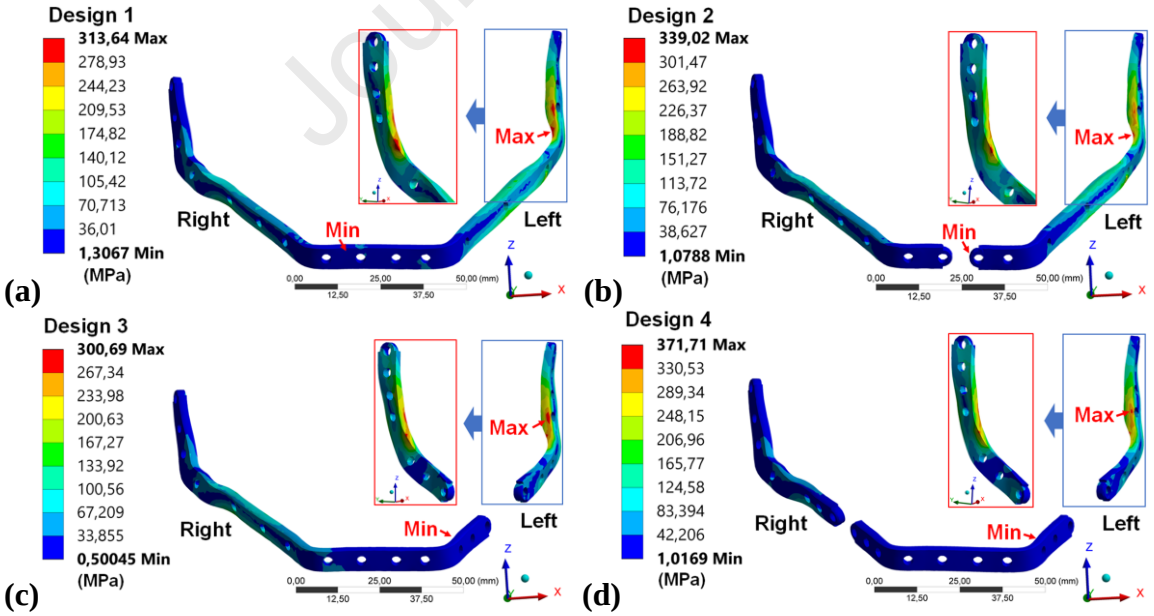

Fig. 8. Von Mises stress distribution on customised MRPs during left molar clenching: (a) Design 1, (b) Design 2, (3) Design 3, and (4) Design 4.

An engineering safety factor (SF), defined as the ratio of the fatigue strength of the Ti-6Al-4V prepared by SLM (510 MPa) to the maximum tensile stress on the MRP [10], was used to evaluate the implant safety.

The SF values of the four designs are summarised in Table 2. Without increasing the thickness and width of the MRPs, the use of a long plate and a short plate (Design 3 [LL61 mm/RL166 mm]) or three short plates (Design 4 [RL61 mm/ML91 mm/RL67 mm]) improves the SF values under both incisor clenching and left molar clenching, compared to Design 1. Moreover, Design 3 reveals the highest SF values among the four designs, showing an SF of 3.52 under incisor clenching and 1.70 under left molar clenching. Interestingly, Design 2 [LL119 mm/RL121 mm], although having two short plates, fails to increase the SF while reducing it to the lowest values of 2.78 and 1.50 under incisor clenching and left molar clenching, respectively. This is a decrease of 15.8% and 8% compared to Design 1 [TL246 mm], respectively. Therefore, it is reasonable to consider that correctly assigning the plate length can be critical to achieving a high SF.

Table 2. Safety factor (SF) of customised MRPs during incisor clenching and left molar clenching.

Designs	Incisor clenching	Left molar clenching
Design 1	3.30	1.63
Design 2	2.78	1.50
Design 3	3.52	1.70
Design 4	3.39	1.37

3.3 Relative displacement between MRPs and mandibles under masticatory activities

Muscle forces can also produce displacement on the mandible and the attached customised MRPs. Maximum total displacement under muscle forces is observed at the left mandible during incisor clenching and at the chin end during left molar clenching, as typically shown by Design 3 [LL61 mm/RL166 mm] (Fig. 9). The value of the maximum total displacement on the MRP and the corresponding mandible in the four designs is summarised in Fig. 10. The left molar clenching can inevitably produce larger total displacements than the incisor clenching due to a larger biting force required. Moreover, the mandible and the attached MRPs move to a different extent under the effect of muscle forces, considering their different material parameters, showing different displacement values. The mandible experiences larger maximum total displacements than the MRPs during incisor clenching (range of 777.9–851.1 μm on the plate *vs.* range of 821.1–889.2 μm on the mandible). In contrast, larger displacements are observed on the MRPs during left molar clenching (range of 1975.7–2134.3 μm on the plate *vs.* range of 1804–2033.7 μm on the mandible). Closer observation reveals that the customised designs with short plates (Designs 2–4) leave larger total displacements than the conventional single long plate in Design 1 [TL246 mm]. Furthermore, the highest total displacement values are seen in Design 3 [LL61 mm/RL166 mm], reaching 2134.3 μm on the plate and 2033.7 μm on the mandible, respectively.

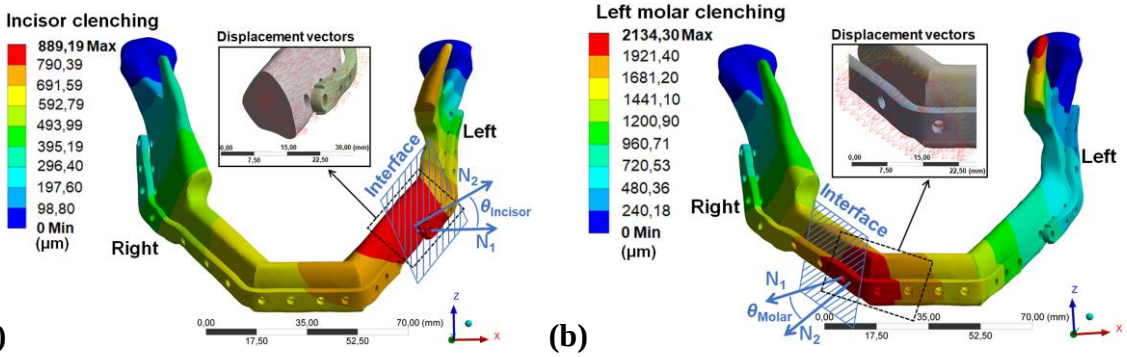

Fig. 9. Total displacement distribution on customised MRPs and the corresponding mandible during (a) incisor clenching and (b) left molar clenching for Design 3. (The insets in (a) and (b) show the displacement vector plots at the region with the largest total displacement to determine the displacement direction N_2. N_1 highlights the axial direction of the screw with the largest relative total displacement.)

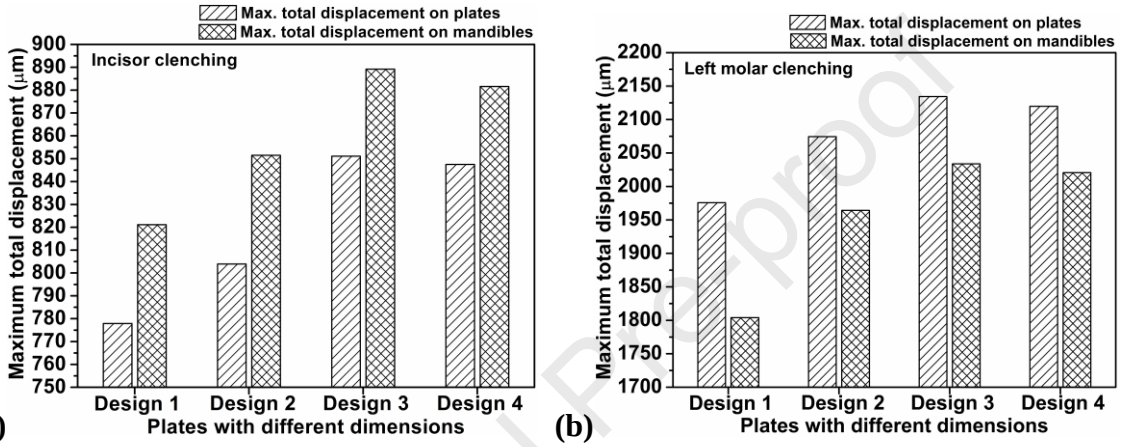

Fig. 10. Maximum total displacement on MRPs and the corresponding mandible during (a) incisor clenching and (b) left molar clenching.

The different magnitudes of displacement on the mandible and the MRP result in relative displacement between them. Compared to the absolute displacement shown in Fig. 9 and Fig. 10, the relative displacement between the components fixed together by screws plays a more significant role in the system fixation stability [38]. That is because the dynamic shear stress on a screw that fixes adjacent components with relative radial displacement is likely to loosen the threaded fastener and even cause bending fracture of the screw. On the other hand, any relative displacement between components that occurs along the axial direction of the screw can cause axial tensile or compressive stress, possibly resulting in a tensile or compressive fracture of the screw and thus impacting fixation stability. Therefore, to gain a detailed understanding of the effects of MRP designs on system fixation stability, the relative total displacement (RD_{Total}) between the MRP and the corresponding mandible must be decomposed into a radial component and an axial component regarding the screw; they are termed as RD_{Radial} and RD_{Axial}, respectively.

The region with the largest total displacement was observed to leave the largest relative total displacement on the screw near the centre of this region (Fig. 9). Therefore, this screw was analysed, as an example, to evaluate the system fixation stability, considering its highest risk of fracturing. Based on the

above observation, RD_{Total} was determined by the difference between the maximum total displacements of the MRP and the corresponding mandible (Fig. 10). The calculated RD_{Total}, RD_{Radial} and RD_{Axial} values are summarised in Fig. 11, following the displacement decomposition strategy illustrated in the inset. N_1 highlights the axial direction of the screw with the largest relative total displacement, and N_2 shows the direction of the displacement, which is determined by the displacement vector plots shown in Fig. 9. Furthermore, Fig. 9 shows an intersection angle between N_1 and N_2 during incisor clenching ($\theta_{Incisor}$) and left molar clenching (θ_{Molar}). For the four designs, $\theta_{Incisor}$ is around 25° and θ_{Molar} is around 20°, suggesting the intersection angle is mainly dependent on the muscle loading condition rather than the implant design. According to the displacement decomposition strategy, RD_{Radial} and RD_{Axial} can be defined by the following. For incisor clenching:

$$RD_{Axial}(\text{Incisor clenching}) = RD_{Total}(\text{Incisor clenching})\cdot\cos\theta_{Incisor} \quad (1)$$

$$RD_{Radial}(\text{Incisor clenching}) = RD_{Total}(\text{Incisor clenching})\cdot\sin\theta_{Incisor} \quad (2)$$

For left molar clenching:

$$RD_{Axial}(\text{Left molar clenching}) = RD_{Total}(\text{Left molar clenching})\cdot\cos\theta_{Molar} \quad (3)$$

$$RD_{Radial}(\text{Left molar clenching}) = RD_{Total}(\text{Left molar clenching})\cdot\sin\theta_{Molar} \quad (4)$$

Relatively higher total displacement on the mandible during incisor clenching leads to RD_{Axial} being antiparallel to N_2 (shown as negative values in Fig. 11), causing axial compressive stress on the screw, while higher total displacement on the MRP during left molar clenching leads to RD_{Axial} being parallel to N_2, leaving axial tensile stress (shown as positive values in Fig. 11). Although there are high total displacements (Fig. 10), the designs with short plates (Designs 2–4) exhibit lower relative displacement values compared to Design 1 (Fig. 11). Especially, the relative total displacement RD_{Total} of Design 3 [LL61 mm/RL166 mm] (100.60 μm) during left molar clenching is 41.4% lower than that of Design 1 [TL246 mm]. The RD_{Axial} and RD_{Radial} of Design 3 are also comparatively low among the four cases.

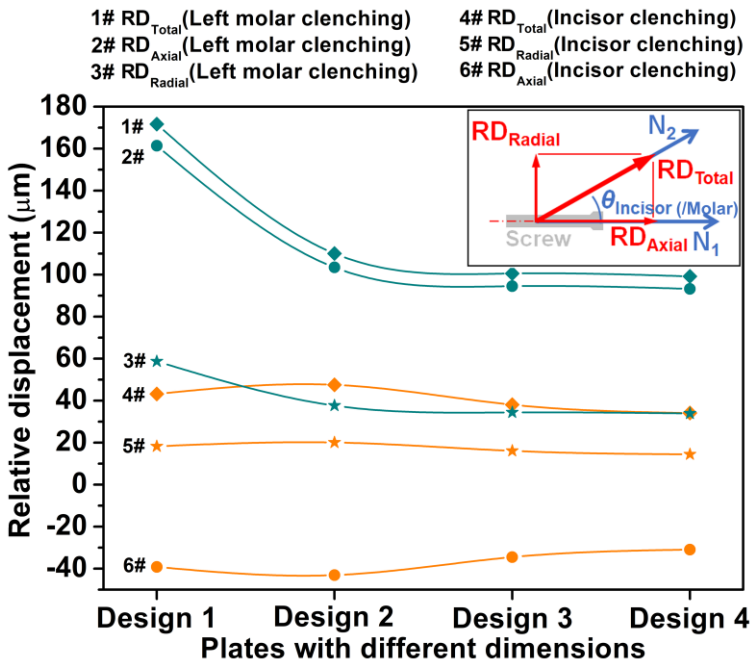

Fig. 11. Calculated relative total displacement (RD_{Total}) and decomposed relative axial displacement (RD_{Axial}) and relative radial displacement (RD_{Radial}) during incisor clenching and left molar clenching. (The inset shows the schematic for decomposing the relative total displacement.)

3.4 Bone segment dislocation under masticatory activities

To understand the bone junction stability provided by the customised MRPs, the bone segment dislocation under masticatory activities was evaluated by the relative displacement between the two sides of a bone junction (L1, L2, L3, and L4 in Fig. 2). The collected dislocation values are summarised in Fig. 12. A low dislocation represents high stability of the bone segments during the mandible reconstruction, benefiting the recovery of bone junctions. During incisor clenching, the greatest bone segment dislocation is observed on Design 4 [RL61 mm/ML91 mm/RL67 mm], up to 20 μm at L4, indicating a comparatively high possibility of dehiscence at the bone junction. Design 3 [LL61 mm/RL166 mm] exhibits the greatest capability for promising bone segment stability, as the lowest bone segment dislocations at L1, L3, and L4 and second-lowest value at L2 can be seen during incisor clenching.

With the biting activity transferred to left molar teeth, all the bone segment dislocation values are increased. Design 2 [LL119 mm/RL121 mm] produces the highest bone segment dislocation values, with a maximum of 42.1 μm at L2, 280% higher than the value (11.08 μm) at the same junction in Design 1 [TL246 mm]. Still, Design 3 [LL61 mm/RL166 mm] provides the best bone segment stability among the three designs with short plates. That is because its dislocation values at all junctions are significantly lower than those in Design 2 [LL119 mm/RL121 mm] and Design 4 [RL61 mm/ML91 mm/RL67 mm], and are only slightly higher than those in Design 1 [TL246 mm]. Therefore, it is reasonable to conclude that Design 3

could provide the stability needed to fix bone segments during mandible reconstruction, benefiting bone recovery.

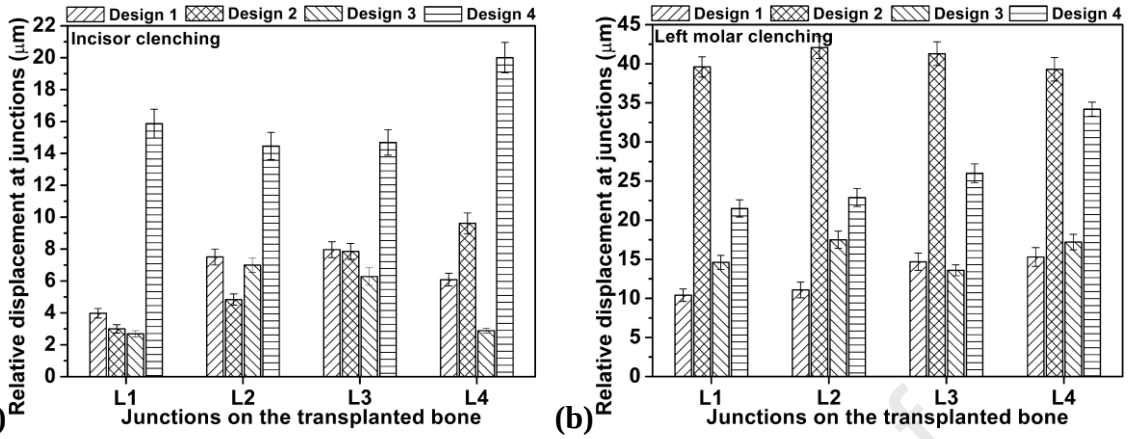

Fig. 12. Relative displacement at bone junctions L1, L2, L3, and L4 during (a) incisor clenching and (b) left molar clenching.

4. Discussion

4.1 Effects of customised MRP designs on implant safety

The effect of differently customised MRP designs on biomechanics is the main focus of this work. This research aims to minimise the implant deformation generated in SLM by shortening the implant length and, at the same time, to guarantee comparable or even superior fixation safety and stability to the conventional single long implant. The maximum von Mises stress on the MRP under incisor clenching (183.2 MPa in Design 2, Fig. 7b) and under left molar clenching (371.71 MPa in Design 4, Fig. 8d) are both lower than 870 MPa (Ti-6Al-4V yield strength from SLM) and 510 MPa (Ti-6Al-4V fatigue strength from SLM), theoretically indicating the safety of customised MRPs during masticatory activities. However, implant fracture is still likely to occur due to metallurgical defects and hydrogen embrittlement induced by biological fluid [10].

This study was performed assuming the bone system is at the late rehabilitation stage, and thus the quantitative data directly reflects the short-term stability of the implant at this stage. On the other hand, the SF was calculated from the fatigue strength that characterises the long-term stability of the material (Table 2). As human masticatory activity can be simplified as repeated cycles of clenching-unclenching, the SF calculated from the fatigue strength can also reflect the implant's long-term stability to some degree. The positive correlation between the SF and the long-term reliability of an engineering part has long been recognised [39]. A high SF enables the reliability of a mechanical device necessary to undertake required the loading during the required time or loading cycles. According to Table 2, it is reasonable to consider that

Design 3 always has the lowest potential to experience implant fracture due to its high SF values under both incisor clenching and left molar clenching.

Note that the implant deformation caused by the SLM process was not considered in the FEA model assembly for the biomechanics simulation. Theoretically, implant deformation can influence the biomechanical behaviour to some degree by changing the relative geometrical position between the MRP and the mandible. However, considering its relatively small deformation range of 1.5–3.7 mm (Fig. 6) compared to the large size of the MRP and mandible (up to 122 mm in one dimension, Fig. 2), the influence can be slight.

In addition, the number and position of screws to fix the MRP onto the mandible is slightly different among the four cases due to clinical preference, as explained in Section 2.2 and Fig. 3. Theoretically, the different screw arrangements would impact the biomechanical results. Fortunately, the MRP designs in this work, including the plate structure and the screw arrangement, initially prioritised both clinical applicability and SLM printability together. Therefore, the biomechanical results could still provide practical information for the design and preparation of short plates by SLM for mandible reconstruction. On the other hand, with a large number of screws, drilling more screw holes on the corresponding bone will inevitably increase the surgical operation time.

4.2 Effects of customised MRP designs on system fixation stability

In addition to the concern about fracture of the MRP itself under the peak stress concentration, another issue is the stability of the MRP fixed on the bone by screws, which is equally critical for the MRP to transfer and share loading under masticatory activities and to guarantee bone healing. Clinical studies have revealed that an unstable MRP in mandible reconstruction has the high potential to cause postoperative complications, such as screw loosening, plate fracture, bone segment dislocation, plate exposure, and infections [23]. Fig. 13 illustrates the screw loosening process during incisor clenching and left molar clenching. To better illustrate the mechanism behind the loss of implant fixation stability under a relative shift between the MRP and the mandible, the screw threads are shown in Fig. 13, although they were simplified in the FEA. In fact, the threaded fastener has an inherent tendency to loosen because of the helical slope on the threads. The upper portion of Fig. 13b shows an enlarged view to highlight the screw reaction, R, to the preload, F_P, at a typical point on a thread. After the fixation of the MRP on the reconstructed mandible during surgery, the system remains stable since the loosening moment developed from the

circumferential component, R_L, can be balanced by the circumferential friction force transferred from the stuck bone-screw interface and plate-screw interface (Fig. 13b). The stuck interface is highlighted by black spots in Fig. 13.

During incisor clenching, RD_{Radial} and negative RD_{Axial} are produced, causing screw bending and compressing (Fig. 13a). However, during left molar clenching, the RD_{Axial} is positive combined with RD_{Radial}, so that the screw bends and stretches (Fig. 13c). It is widely acknowledged that the stress concentration at the thread tip can be easily formed considering its sharp-angled effect, probably resulting in a plastic strain of the thread tip after a certain number of loading-unloading cycles. Furthermore, the strain on the thread could occur at positions with compressive stress during screw bending, as highlighted by the orange rectangles in Fig. 13; consequently, the bone-screw interface and plate-screw interface at the opposite sides of the deformed thread are separated, as highlighted by red triangles. Biomechanically, excessive compression on the edge of screw holes on the bone can cause abrasion losses, as highlighted by the red oval in Fig. 13. The loss of bone further increases the bone-screw interface separation. With the increase in the separated thread interface, the circumferential friction force reduces. As a result, the screw turns loose, forming a so-called 'localised thread slip' [38] and lowering the fixation stability. On the other hand, the fracture of the screw itself by screw bending, compressing and stretching is also a key factor that can impact the system fixation stability, especially considering that the fatigue strength of titanium can be dramatically decreased with the increase of loading-unloading cycles [40]. In this study, Fig. 11 reveals much lower RD_{Total}, RD_{Axial} and RD_{Radial} on the customised MRP designs with short plates (Design 3 [LL61 mm/RL166 mm] and Design 4 [RL61 mm/ML91 mm/RL67 mm]) than on the conventional single long plate in Design 1 [TL246 mm], indicating lower risk of 'localised thread slip'. Therefore, it is reasonable to consider that the short MRPs could provide higher fixation stability than the conventional single long plate in mandible reconstruction.

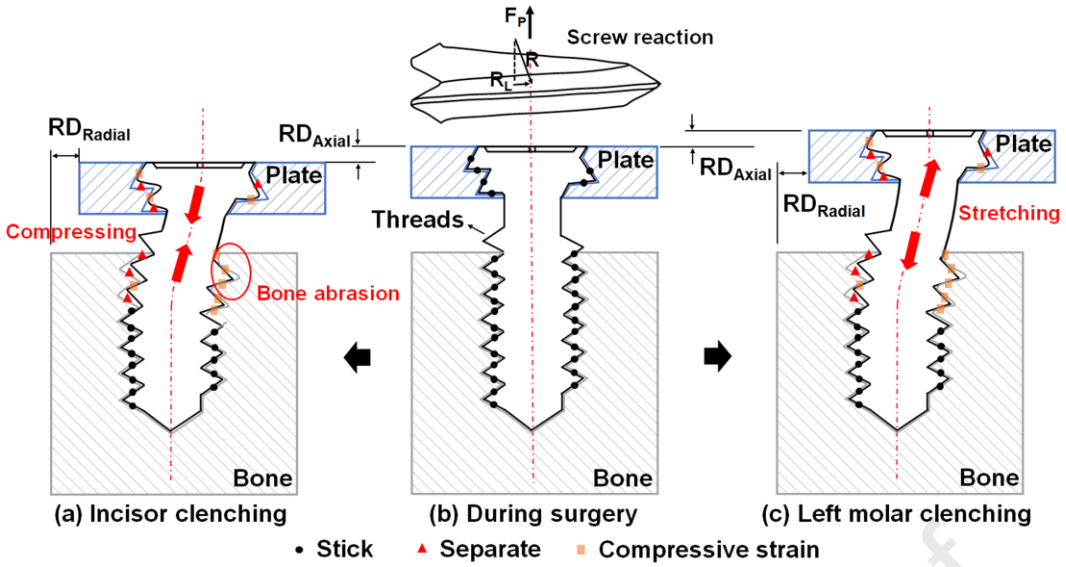

Fig. 13. Screw loosening process during masticatory activities: (a) screw loosening during incisor clenching, (b) no screw loosening during surgery, and (c) screw loosening during left molar clenching.

4.3 Effects of customised MRP designs on bone segment stability

Many experimental and clinical studies have evaluated the efficiency of different fixation systems in mandible reconstruction. However, most of them only paid attention to safe fixation to avoid premature fracture of MRP. This can be accomplished by simulating the peak tensile stress on the plate during masticatory activities and comparing it with the material fatigue strength [26]. Nevertheless, adequate fixation stability and rigidity were typically not considered. A bone segment dislocation greater than 150 μm is clinically considered to lack stability, potentially resulting in nonunion or bone infection [41]. Although in this study there are different bone segment dislocation values at various junctions (Fig. 12), the dislocations in the customised four designs do not exceed the criteria value of 150 μm. Furthermore, Design 3 [LL61 mm/RL166 mm] reveals the lowest dislocation values for the three designs with short plates. The bone segment dislocation values of Design 3 [LL61 mm/RL166 mm] are even lower than the conventional design (Design 1 [TL246 mm]) under incisor clenching and are comparable under left molar clenching. This indicates that using a combination of a long plate and a short plate (Design 3 [LL61 mm/RL166 mm]) to replace a conventional single long plate (Design 1 [TL246 mm]) can provide greater bone fixation stability to aid the bone healing process. However, it should also be noted that the plate length needs to be considered carefully during MRP design, since an inappropriate plate length assignment may fail to lower the bone segment dislocation, as reflected by Design 2 [LL119 mm/RL121 mm] and Design 4 [RL61 mm/ML91 mm/RL67 mm] having much higher bone segment dislocations than the conventional Design 1 [TL246 mm]. On the other hand, the screw hole arrangement inevitably tends to be denser when the plate is too short. The

dense distribution of screw holes on the corresponding bone may cause bone cracks when the screw is squeezed into the screw hole, due to the excessive loss of bone volume locally. Therefore, careful consideration is needed of the trade-off between plate length, bone safety, and implant fixation stability.

5. Conclusions

The biomechanical feasibility of a combination of short MRPs to replace a conventional single long plate for complete mandible reconstruction was preclinically assessed. The following are the main conclusions of this study.

(1) Implant deformation generated during the SLM can be reduced by 30% to 59% on the short MRPs, decreasing the maximum displacement to 1.5–2.6 mm on Designs 2–4 from 3.7 mm on Design 1. The reduced implant deformation could increase the implant placement precision and thus benefit clinical outcomes.

(2) The combination of a long plate and a short plate (Design 3) shows superior biomechanical properties to having a conventional single long plate (Design 1) and reveals the most reliable fixation stability among the three designs with short plates (Designs 2–4). Compared to the conventional Design 1, Design 3 provides higher plate safety (maximum tensile stress on plates reduced by 6.3%), lower system fixation instability (relative total displacement reduced by 41.4%), and good bone segment stability (bone segment dislocation below 42.1μm) under masticatory activities. Therefore, the biomechanical feasibility and fixation stability of using short MRPs for complete mandible reconstruction can be preclinically demonstrated. Notedly, plate length should be carefully designed to obtain reliable biomechanical properties.

(3) The results in this work are expected to provide valuable information for the treatment of other large-sized bone defects using short, customised implants, expanding the potential of additive manufacturing in implant applications.

(4) Randomised clinical trials and in vivo investigations are suggested to verify the actual clinical performance and usefulness of using short SLM-fabricated MRPs for complete mandible reconstruction.

Acknowledgements

The authors gratefully acknowledge the help in manuscript revision from Dr Robin Willaert, Department of Oral and Maxillofacial Surgery, University Hospitals Leuven, Belgium. The author, Qimin Shi, also appreciates the financial support from the China Scholarship Council (No. 201806830109).

References

[1] Y. Yao, Z. Mo, G. Wu, J. Guo, J. Li, L. Wang, Y. Fan, A personalized 3D-printed plate for tibiotalocalcaneal arthrodesis: Design, fabrication, biomechanical evaluation and postoperative assessment, Comput. Biol. Med. 133 (2021) 104368. https://doi.org/10.1016/j.compbiomed.2021.104368
[2] A. Dutta, K. Mukherjee, S. Dhara, S. Gupta, Design of porous titanium scaffold for complete mandibular reconstruction: The influence of pore architecture parameters, Comput. Biol. Med. 108 (2019) 31-41. https://doi.org/10.1016/j.compbiomed.2019.03.004
[3] H. Wang, J.Y. Lim, Metal-ceramic bond strength of a cobalt chromium alloy for dental prosthetic restorations with a porous structure using metal 3D printing, Comput. Biol. Med. 112 (2019) 103364. https://doi.org/10.1016/j.compbiomed.2019.103364
[4] A. Chakraborty, P. Datta, S. Majumder, S.C. Mondal, A. Roychowdhury, Finite element and experimental analysis to select patient's bone condition specific porous dental implant, fabricated using additive manufacturing, Comput. Biol. Med. 124 (2020) 103839. https://doi.org/10.1016/j.compbiomed.2020.103839
[5] D. Gu, X. Shi, R. Poprawe, D.L. Bourell, R. Setchi, J. Zhu, Material-structure-performance integrated laser-metal additive manufacturing, Science 372 (2021) eabg1487. https://doi.org/10.1126/science.abg1487
[6] A.M.C. Goodson, S. Parmar, S. Ganesh, D. Zakai, A. Shafi, C. Wicks, R. O'Connor, E. Yeung, F. Khalid, A. Tahim, S. Gowrishankar, A. Hills, E.M. Williams, Printed titanium implants in UK cranio-maxillofacial surgery: Part II – perceived performance (outcomes, logistics and costs), Br. J. Oral Maxillofac. Surg. (2020) YBJOM 6243. https://doi.org/10.1016/j.bjoms.2020.08.088
[7] J.E. Bechtold, Application of computer graphics in the design of custom orthopedic implants, Orthop. Clin. North Am. 17 (1986) 605-612. https://doi.org/10.1016/S0030-5898(20)32307-5
[8] D. Gu, W. Meiners, K. Wissenbach, R. Poprawe, Laser additive manufacturing of metallic components: materials, processes and mechanisms, Int. Mater. Rev. 57 (2012) 133-164. https://doi.org/10.1179/1743280411y.0000000014
[9] A.A. Almansoori, H.-W. Choung, B. Kim, J.-Y. Park, S.-M. Kim, J.-H. Lee, Fracture of standard titanium mandibular reconstruction plates and preliminary study of three-dimensional printed reconstruction plates, J. Craniomaxillofac. Surg. 78 (2020) 153-166. https://doi.org/10.1016/j.joms.2019.07.016
[10] Q. Shi, Y. Sun, S. Yang, J. Van Dessel, H.-T. Lübbers, S. Zhong, Y. Gu, M. Bila, T. Dormaar, J. Schoenaers, C. Politis, Failure analysis of an in-vivo fractured patient-specific Ti6Al4V mandible reconstruction plate fabricated by selective laser melting, Eng. Fail. Anal. 124 (2021) 105353. https://doi.org/10.1016/j.engfailanal.2021.105353
[11] P. Mercelis, J.P. Kruth, Residual stresses in selective laser sintering and selective laser melting, Rapid Prototyp. J. 12 (2006) 254-265. https://doi.org/10.1108/13552540610707013
[12] C. Li, J.F. Liu, X.Y. Fang, Y.B. Guo, Efficient predictive model of part distortion and residual stress in selective laser melting, Addit. Manuf. 17 (2017) 157-168. https://doi.org/10.1016/j.addma.2017.08.014
[13] E. Ellis, C. Price, Treatment protocol for fractures of the atrophic mandible, J. Oral Maxillofac. Surg. 66 (2008) 421-435. https://doi.org/10.1016/j.joms.2007.08.042
[14] A. Ahmed, A. Majeed, Z. Atta, G. Jia, Dimensional quality and distortion analysis of thin-walled alloy parts of AlSi10Mg manufactured by selective laser melting, J. Manuf. Mater. Process. 3 (2019) https://doi.org/10.3390/jmmp3020051
[15] L. Palka, V. Konstantinovic, P. Pruszynski, K. Jamroziak, Analysis using the finite element method of a novel modular system of additively manufactured osteofixation plates for mandibular fractures - A preclinical study, Biomed. Signal. Process. Control. 65 (2021) 102342. https://doi.org/10.1016/j.bspc.2020.102342
[16] T. Barbin, D.V. Velôso, L. Del Rio Silva, G.A. Borges, A.G.C. Presotto, V.A.R. Barão, M.F. Mesquita, 3D metal printing in dentistry: An in vitro biomechanical comparative study of two additive manufacturing technologies for full-arch implant-supported prostheses, J. Mech. Behav. Biomed. Mater. 108 (2020) 103821. https://doi.org/10.1016/j.jmbbm.2020.103821
[17] R. Xiao, X. Feng, R. Fan, S. Chen, J. Song, L. Gao, Y. Lu, 3D printing of titanium-coated gradient composite lattices for lightweight mandibular prosthesis, Compos. B. Eng. 193 (2020) 108057. https://doi.org/10.1016/j.compositesb.2020.108057
[18] X. Pei, L. Wu, H. Lei, C. Zhou, H. Fan, Z. Li, B. Zhang, H. Sun, X. Gui, Q. Jiang, Y. Fan, X. Zhang, Fabrication of customized Ti6AI4V heterogeneous scaffolds with selective laser melting: Optimization of the architecture for orthopedic implant applications, Acta Biomater. 126 (2021) 485-495. https://doi.org/10.1016/j.actbio.2021.03.040
[19] S. Lee, W. Zhu, L. Heyburn, M. Nowicki, B. Harris, L.G. Zhang, Development of novel 3-D printed scaffolds with core-shell nanoparticles for nerve regeneration, IEEE Trans. Biomed. Eng. 64 (2017) 408-418. https://doi.org/10.1109/tbme.2016.2558493
[20] A.A. Guy, A.W. Justin, D.M. Aguilar-Garza, A.E. Markaki, 3D printable vascular networks generated by accelerated constrained constructive optimization for tissue engineering, IEEE Trans. Biomed. Eng. 67 (2020) 1650-1663. https://doi.org/10.1109/tbme.2019.2942313
[21] P. Szypryt, D. Forward, The use and abuse of locking plates, Orthopaedics and Trauma 23 (2009) 281-290. https://doi.org/10.1016/j.mporth.2009.07.002
[22] S. Zhong, Q. Shi, Y. Sun, S. Yang, J. Van Dessel, Y. Gu, X. Chen, H.-T. Lübbers, C. Politis, Biomechanical comparison of locking and non-locking patient-specific mandibular reconstruction plate using finite element analysis, J. Mech. Behav. Biomed. Mater. 124 (2021) 104849. https://doi.org/10.1016/j.jmbbm.2021.104849

[23] A. Kimura, T. Nagasao, T. Kaneko, T. Tamaki, J. Miyamoto, T. Nakajima, Adaquate fixation of plates for stability during mandibular reconstruction, J. Craniomaxillofac. Surg. 34 (2006) 193-200. https://doi.org/10.1016/j.jcms.2006.01.003
[24] J. Wang, Y. Liu, C.D. Rabadia, S.-X. Liang, T.B. Sercombe, L.-C. Zhang, Microstructural homogeneity and mechanical behavior of a selective laser melted Ti-35Nb alloy produced from an elemental powder mixture, J. Mater. Sci. Technol. 61 (2021) 221-233. https://doi.org/10.1016/j.jmst.2020.05.052
[25] P. Qi, B. Li, T. Wang, L. Zhou, Z. Nie, Evolution of microstructural homogeneity in novel Ti-6Zr-5Fe alloy fabricated by selective laser melting, Mater. Charact. 171 (2021) 110729. https://doi.org/10.1016/j.matchar.2020.110729
[26] M. Pinheiro, J.L. Alves, The feasibility of a custom-made endoprosthesis in mandibular reconstruction: Implant design and finite element analysis, J. Craniomaxillofac. Surg. 43 (2015) 2116-2128. https://doi.org/10.1016/j.jcms.2015.10.004
[27] E. Wycisk, C. Emmelmann, S. Siddique, F. Walther, High cycle fatigue (HCF) performance of Ti-6Al-4V alloy processed by selective laser melting, Adv. Mat. Res. 816-817 (2013) 134-139. https://doi.org/10.4028/www.scientific.net/AMR.816-817.134
[28] X. Yan, S. Yin, C. Chen, C. Huang, R. Bolot, R. Lupoi, M. Kuang, W. Ma, C. Coddet, H. Liao, M. Liu, Effect of heat treatment on the phase transformation and mechanical properties of Ti6Al4V fabricated by selective laser melting, J. Alloys Compd. 764 (2018) 1056-1071. https://doi.org/10.1016/j.jallcom.2018.06.076
[29] S. Prasadh, S. Suresh, K.L. Hong, A. Bhargav, V. Rosa, R.C.W. Wong, Biomechanics of alloplastic mandible reconstruction using biomaterials: The effect of implant design on stress concentration influences choice of material, J. Mech. Behav. Biomed. Mater. 103 (2020) 103548. https://doi.org/10.1016/j.jmbbm.2019.103548
[30] Y.-f. Liu, Y.-y. Fan, H.-y. Dong, J.-x. Zhang, An investigation of two finite element modeling solutions for biomechanical simulation using a case study of a mandibular bone, J. Biomech. Eng. 139 (2017) https://doi.org/10.1115/1.4037633
[31] K.L. Andersen, E.H. Pedersen, B. Melsen, Material parameters and stress profiles within the periodontal ligament, Am. J. Orthod. Dentofacial Orthop. 99 (1991) 427-440. https://doi.org/10.1016/S0889-5406(05)81576-8
[32] R.H. Haug, C.C. Street, M. Goltz, Does plate adaptation affect stability? A biomechanical comparison of locking and nonlocking plates, J. Oral Maxillofac. Surg. 60 (2002) 1319-1326. https://doi.org/10.1053/joms.2002.35732
[33] N. Narra, J. Valášek, M. Hannula, P. Marcián, G.K. Sándor, J. Hyttinen, J. Wolff, Finite element analysis of customized reconstruction plates for mandibular continuity defect therapy, J. Biomech. 47 (2014) 264-268. https://doi.org/10.1016/j.jbiomech.2013.11.016
[34] T.W.P. Korioth, D.P. Romilly, A.G. Hannam, Three-dimensional finite element stress analysis of the dentate human mandible, Am. J. Phys. Anthropol. 88 (1992) 69-96. https://doi.org/10.1002/ajpa.1330880107
[35] T.W.P. Korioth, A.G. Hannam, Deformation of the human mandible during simulated tooth clenching, J. Dent. Res. 73 (1994) 56-66. https://doi.org/10.1177/00220345940730010801
[36] Q. Shi, D. Gu, M. Xia, S. Cao, T. Rong, Effects of laser processing parameters on thermal behavior and melting/solidification mechanism during selective laser melting of TiC/Inconel 718 composites, Opt. Laser. Technol. 84 (2016) 9-22. https://doi.org/10.1016/j.optlastec.2016.04.009
[37] L.M. Ritschl, A.M. Fichter, F.D. Grill, D. Hart, A. Hapfelmeier, H. Deppe, D.M. Hedderich, K.-D. Wolff, T. Mücke, Bone volume change following vascularized free bone flap reconstruction of the mandible, J. Craniomaxillofac. Surg. 48 (2020) 859-867. https://doi.org/10.1016/j.jcms.2020.07.011
[38] N.G. Pai, D.P. Hess, Three-dimensional finite element analysis of threaded fastener loosening due to dynamic shear load, Eng. Fail. Anal. 9 (2002) 383-402. https://doi.org/10.1016/S1350-6307(01)00024-3
[39] M. Dao-Thien, M. Massoud, On the relation between the factor of safety and reliability, J. Eng. Ind. 96 (1974) 853-857. https://doi.org/10.1115/1.3438452
[40] L. Du, G. Qian, L. Zheng, Y. Hong, Influence of processing parameters of selective laser melting on high-cycle and very-high-cycle fatigue behaviour of Ti-6Al-4V, Fatigue Fract. Eng. M. 44 (2021) 240-256. https://doi.org/10.1111/ffe.13361
[41] A. Vajgel, I.B. Camargo, R.B. Willmersdorf, T.M. de Melo, J.R.L. Filho, R.J. de Holanda Vasconcellos, Comparative finite element analysis of the biomechanical stability of 2.0 fixation plates in atrophic mandibular fractures, J. Oral Maxillofac. Surg. 71 (2013) 335-342. https://doi.org/10.1016/j.joms.2012.09.019

Highlights

- Biomechanics of short plates for complete mandible reconstruction was studied.
- Implant deformation caused by 3D printing was predicted to assist plate design.
- Specific short plates combination has superior biomechanics to a single long plate.
- Short plates can be biomechanically feasible to treat large-sized bone defects.

Declaration of interests

☒ The authors declare that they have no known competing financial interests or personal relationships that could have appeared to influence the work reported in this paper.

☐The authors declare the following financial interests/personal relationships which may be considered as potential competing interests: